Type of contribution:
Editorial
▶ Research Paper
Case Study
Review Paper
Scientific Data
Report of Tech. Application

mesi
e-issn. 2798-5245

Mechanical Engineering for Society and Industry
Vol. 3, No. 2 (2023) pp 93-104
https://doi.org/10.31603/mesi.10365

Thermodynamic modelling of a novel solar-ORC with bottoming ammonia-water absorption cycle (SORCAS) powered by a vapour compression refrigeration condensate for combined cooling and power

Fidelis Ibiang Abam[1], Macmanus Chinenye Ndukwu[2], Oliver Ibor Inah[3], Onyishi Donatus Uchechukwu[4], Muji Setiyo[5,6], Olusegun David Samuel[7] *, Remy Uche[8]

[1] Energy, Exergy and Environment Research Group (EEERG), Department of Mechanical Engineering, University of Calabar, **Nigeria**
[2] Department of Agricultural and Bioresources Engineering, Michael Okpara University of Agriculture Umudike, **Nigeria**
[3] Department of Mechanical Engineering, University of Cross River State, Calabar, **Nigeria**
[4] Department of Electrical and Electronics Engineering, Federal University of Petroleum Resources, Effurun, P.M.B 1221, Delta State, **Nigeria**
[5] Department of Mechanical Engineering, Universitas Muhammadiyah Magelang, **Indonesia**
[6] Center of Energy Studies for Society and Industry (CESI), Universitas Muhammadiyah Magelang, **Indonesia**
[7] Department of Mechanical Engineering, Federal University of Petroleum Resources, Effurun, P.M.B 1221, Delta State, **Nigeria**
[8] Department of Mechanical Engineering, Federal University of Technology Owerri, **Nigeria**
✉ samuel.david@fupre.edu.ng

This article contributes to:

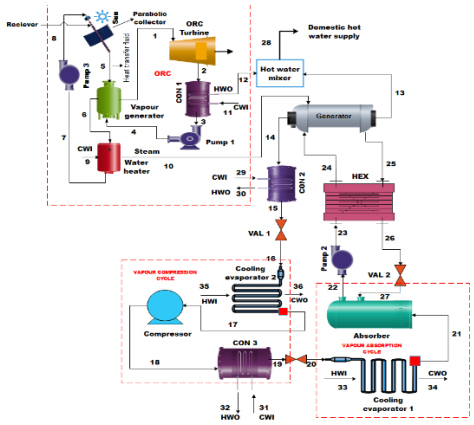

Highlights:

- The overall refrigerating effect and COP were calculated at 1358 kW and 2.34 respectively
- The cooling rate increases for increasing generator temperature by 1.73%.
- The energy and exergy efficiencies for the ORC topping cycle were 21.44 and 45%, respectively.
- The system's estimated total improvement potential was 426.768 kW.

Article info

Submitted: 2023-10-13
Revised: 2023-11-24
Accepted: 2023-11-26

Publisher
Universitas Muhammadiyah Magelang

Abstract

The current study proposed an innovative combined power and cooling solar Organic Rankine Cycle (ORC) with bottoming vapour absorption (VAS) and vapour compression refrigeration (VCP) cycles using ammonia–water as the working fluid. The advantage of these cycles is the integration of two cooling evaporators, producing equivalent refrigerating effects from the VCP condensate. The power generation sub-system, the topping cycle, employed a solar-driven ORC. At operating conditions, the energy and exergy efficiencies stood at 38.63 and 42.09%, respectively, with overall refrigerating effect, power output, and COP calculated at 1358 kW, 26.65 kW, and 2.34 in that order. The parametric results indicated a 40% and 55% increase in energy and exergy efficiencies at high turbine inlet temperatures, with a 1.73% increase in refrigerating effect and a 1.56% decrease in the exergy of cooling. Similarly, at an elevated generator pressure of 4.75 bar, an overall COP of 3.046 was reached. The total exergy of products and fuel was calculated at 1347.91 and 786.38 kW, respectively, with an exergy destruction ratio of 0.997. The results showed a total improvement potential (IP) of 426.768 kW, with the evaporators, absorber, and heat exchanger having the highest IP of 66. 32, 119.4, and 68.08 kW respectively. The study showed enhancement in performance when compared with previous studies and recommended system optimization and sustainability analysis as future considerations for system practical application.

Keywords: Solar-ORC; Ammonia-water; Exergy; Energy; COP

Nomenclature	
A_a	Aperture plane area (m^2)
A_r	Receiver area (m^2)
$D_{r,0\ and\ D_{r,i}}$	Receiver tube outside and inside diameter (mm)
$\dot{F}$	Efficiency factor (%)
G_B	Total incident radiation (W/m^2)
h	Enthalpy (kJ/kg)
h_{fi}	Convective heat transfer coefficient
k_r	Thermal conductivity of the receiver tube (W/m K)
U_0	Overall heat transfer coefficient ($W/m^2/K$)

1. Introduction

Binary mixtures display mutable boiling points or temperatures during the boiling progression, making them apt to finite heat sources. The specific utilization of ammonia with water as a binary mixture has numerous advantages. Water and ammonia have comparable molecular weights, while the boiling point of ammonia is significantly smaller, making it practically suitable to be employed in low-heat temperature systems [1], [2]. Additionally, with the global utilization of conventional fuels and following the environmental consequences, substantial attention has been drawn to the expansion and use of low-grade heat sources and renewable energy, including solar energy, waste heat from the industry, and geothermal heat resources [3]. Between the different utilization techniques, the combined power and cooling plants show remarkable energy transfer efficiency, making it a promising technology to deliver both refrigerating outputs and power concurrently.

Several studies exist regarding the combined power and cooling system employing ammonia-water as a working fluid. Studies [4], [5] suggested a novel combined power system for power and cooling production concurrently with a single heat source. Goswami and Xu [6] and Goswami and Xu [7] suggested enhancing the Goswami cycle (GOC) by incorporating a superheater between the turbine and condenser/rectifier to increase the turbine's inlet temperature and increase power production. The effects of variations in heat source temperature, boiler pressures, ammonia concentrations, and turbine isentropic efficiency on power production, cooling rate, and GOC effective efficiencies were also examined by Kim et al. [8]. The effects of a few significant performance characteristics on the GOC's operation were examined by Yu et al. [9]. The results revealed that increased inlet turbine pressure decreases system output power. Analogously, A Kalina-based cycle (KC), including a pre-cooler and an ammonia-water absorption refrigeration cycle (ARC) was proposed by Jing [10]. A unique combined power and cooling cycle was proposed by Hua et al. [11] by the integration of a dual-effect ammonia–water vapour absorption refrigeration system with a KC. They investigated the impact of cycle coupling- arrangement on energy cascade consumption. Furthermore, Sun et al. [12] included a sub-cooler and an evaporator to a KC to develop an ammonia-water power-cooling system using low-grade waste heat whereas Sun et al. [13] proposed a novel ammonia-water power-cooling cogeneration cycle using low-temperature heat comprising an ORC and an ARC. The waste heat from the high-temperature part was utilized mainly for power generation, while the low-temperature portion was for cooling production. The study obtained energy and exergy efficiencies of 40.6% and 36.4%, respectively, with a maximum cooling rate of 13 kW at turbine inlet pressure of 32 bar. Han et al. [14] developed a cogeneration cycle that utilized the exhaust vapour from the turbine to chill ammonia and water in a different investigation. The strong ammonia-water concentration unit of the cycle was designed using an adjustable system. The results obtained a cooling rate of 11.67 kW, with a COP and conversion efficiency of 0.465 and 3.98%, respectively. An inventive cooling-power cogeneration system was presented by Shankar and Srinivas [15], in which the working fluid (ammonia-water) condenses at the turbine's exit towards the saturated liquid phase. The latter enhances the cooling rate of the entire cycle. Mendoza et al. [16] proposed a novel solo-stage integrated absorption power-cooling cycle with double sub-cyclic processes whereas López-Villada et al. [17] presented a solar-based adsorption power-cooling Goswami Cycle for different mixtures of NH_3/H_2O, $NH_3/LiNO_3$ and $NH_3/NaSCN$. For the power-cooling cycle using NH_3/H_2O, the monthly efficiency obtained ranged between 30 and 50%, with yearly average cooling energy not exceeding 25 MWh. From the examined literature, one major drawback of the studied cycles is the low cooling production rate and long pathway of working fluids to the end state for conversion. Besides, to narrow this gap, this study developed a novel bottoming ammonia-water vapour-

absorption system (VAS) powered by the refrigerant condensate from the vapour compression cycle (VCP). In this case, the utilization potential of the ammonia-vapour exiting the VAS generator is first condensed, throttled to reduce the pressure and temperature without compression and then allowed to evaporate in evaporator 1 (EVP1), producing cooling. The evaporated vapour from EVP 1 is compressed in the VCP system to increase the kinetic energy and further re-condensed, re-throttled and allowed to evaporate in EVP 2, thus producing an equivalent refrigerating effect in the VAS. The same working fluid is used to achieve an equivalent refrigerating effect, thus increasing the overall cooling capacity, and reducing the working fluid's thermodynamic pathways before conversion. The latter is the main novelty of the developed system based on the configuration. However, the mathematical simulation and thermodynamic analysis are performed to estimate the practicability of the proposed system. Thermal and exergy efficiencies are employed as performance measures to observe the influence of some important thermodynamic parameters on the system performance. Also, the exergy destruction breakdown is carried out to qualitatively ascertain the irreversibilities in the system components.

2. Methods

2.1. System Description

Figure 1 depicts the proposed energy system that comprises an ORC system driven by solar irradiation, a domestic water heater, and a single-effect bi-evaporator refrigeration system. The primary energy input to the system is from a solar collector, which exchanges heat via a vapour generator for driving the ORC and further heats up a domestic water heater for steam generation for driving the vapour absorption system for refrigeration. A separate working fluid is provided for the solar heating continuously pumped through the ORC vapour generator and domestic water. In the ORC, the vapour generator heats up the working fluid, which expands in the turbine producing power. This is then condensed and pumped back to the vapour generator for the next cycle. The vapour absorption system is driven by steam from the solar energy stream after the ORC vapour generator. It is mixed with hot water produced from the ORC condenser. The two streams are mixed for domestic hot water production. In the vapour absorption system, the generator heats up ammonium water solution to the required generator temperature, freeing a rich ammonia vapour and allowing it to condense in condenser 2, throttled and evaporate in EVP1 to produce cooling. The vapour from EVP1 is compressed and condensed in condenser 3. The condensate is throttled and allowed to evaporate in EVP 2 on the VAS side, thus producing an equivalent cooling effect. The absorber receives this stream and mixes with the weak ammonium water solution. Water is provided in the absorber to enable a large amount of ammonia absorption, thus forming a rich aqua ammonia solution pumped via a heat exchanger to the generator for another cycle.

2.2. System Modelling

For system simulation, the mathematical models describing the proposed combined power-cooling system are first established and built on thermodynamics' mass and conservation principles, momentum, and energy laws. Furthermore, to streamline the mathematical models, the following assumptions are made: (1)The operation of the system exists at a steady state condition, (2) The drops in pressure across all the system components are neglected, (3) No heat transfer across and between the system boundaries, (4) the working fluid vapour and water vapour leaving the generator are all saturated, (5) the assumed heat source for this study is solar energy, (6) the system working fluid temperature is cooled to saturation in the condenser, and the fluid flow across the throttle valves is at constant enthalpy. The developed system will also be simulated under varying operating settings, with a developed computational program based on EES (Engineering Equation Solver) simulator software. The Ammonia-water mix properties in the absorption system are obtainable in the EES data collection and integrated into the simulation platform.

2.3. Energy Balances

The general energy flow balance for a thermodynamic system under steady state for the k^{th} component is obtained in Eq. (1) Ozlu and Dincer [18].

$$\sum \dot{Q}_k + \sum \dot{m}_i \left(h_1 + \frac{C_i^2}{2} + gz_1 \right) = \sum \dot{m}_e \left(h_2 + \frac{C_0^2}{2} + gz_2 \right) + \sum W \quad (1)$$

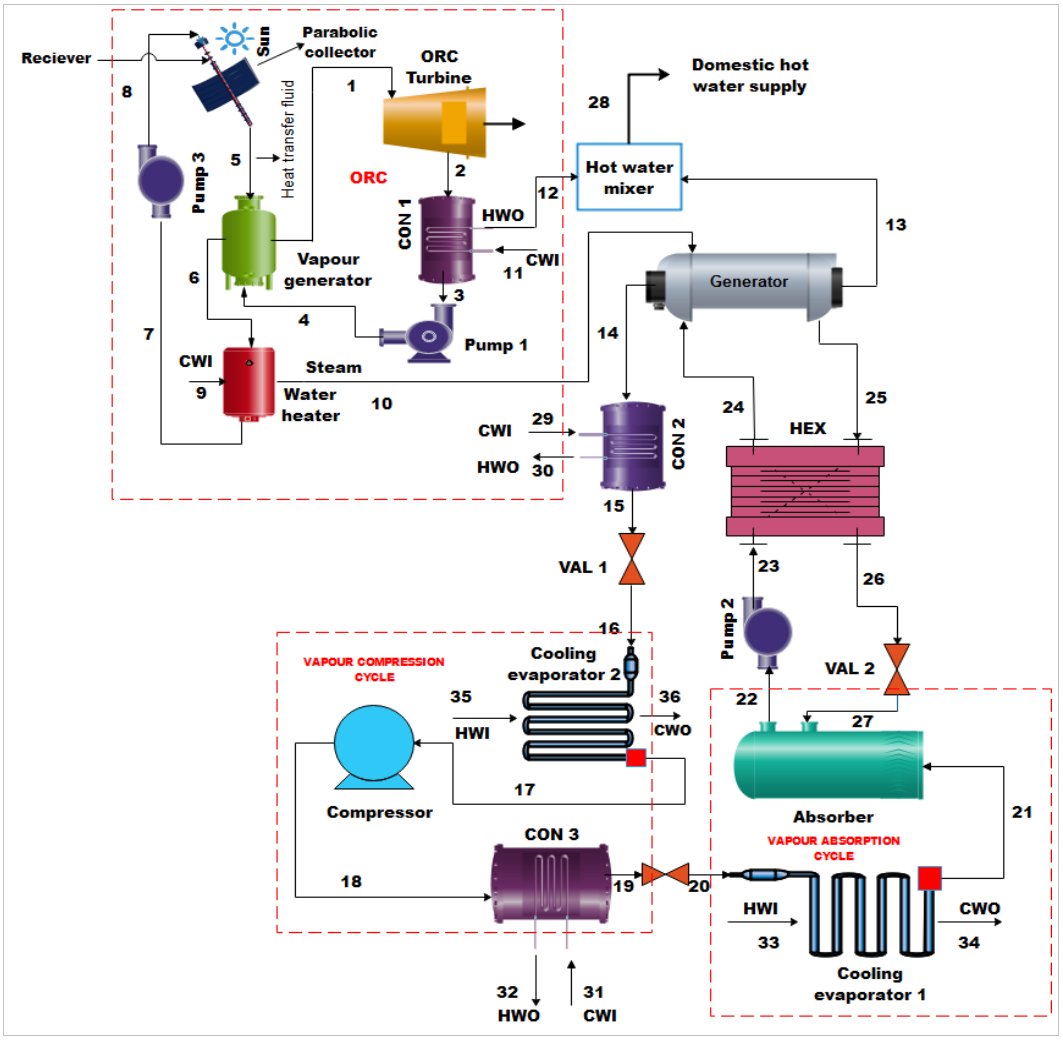

Figure 1. Schematic of the new integrated solar power-cooling ammonia–water cycle

The useful energy delivered from the parabolic solar collector (PSC) is given by Eq. (2)

$$Q_u = \dot{m}_8 Cp_8 (T_8 - T_5) \tag{2}$$

where, Cp_8 T_8, T_5 and $\dot{m}_8$ signify the specific heat of thermal oil, solar collector outlet temperature, inlet temperature and mass flow rate of the thermal oil in the receiver, respectively. The $C_{pavg} = Cp_8$ obtained at $T_{ave} = \frac{1}{2}(T_8 + T_5)$. Similarly, the useful energy can also be evaluated by Ozlu and Dincer [18] as:

$$Q_u = F_R[G_B \eta_0 A_a - A_r U_L (T_8 - T_{amb})] \tag{3}$$

F_R is calculated from Eq. (4).

$$F_R = \frac{\dot{m}_{to} Cp_{to}}{A_r U_L}\left[1 - exp\left(-\frac{U_L \acute{F} A_r}{\dot{m}_{to} Cp_{to}}\right)\right] \tag{4}$$

$$\acute{F} = \frac{\frac{1}{U_L}}{\frac{1}{U_L} + \frac{D_{r,0}}{h_{fi} D_{r,i}} + \left(\frac{D_{r,0}}{2\,k_r} ln \frac{D_{r,0}}{D_{r,i}}\right)} = \frac{U_0}{U_L} \tag{5}$$

$$\eta_c = \frac{Q_u}{A_a G_B} \tag{6}$$

Eq. (1) was used to develop all the energy balances in the component systems. The major performance parameter for the subsystem is presented as follows:

a. Energy efficiency of the ORC subsystem

$$\eta_{ef} = \frac{\dot{W}_{ORC,tubine} - \dot{W}_{ORC,pump}}{Q_{in}} \tag{7}$$

b. The coefficient of performance

The coefficient of performance is defined for the two cooling subsystems (a) the EVP1 in the VCP side and (b) the EVP2 in the VAS side. The COP in the VCP side is presented in Eq. (8).

$$COP_{VCP} = \frac{Q_{EVP1}}{\dot{m}_{13}(h_{13} - h_{10})} \tag{8}$$

where $\dot{m}_{13}(h_{13} - h_{10})$ is the energy input for the $\dot{Q}_{gen}$ since the system is design different from the convention type. Here what drives cooling (**Figure 1**) is the energy from $\dot{Q}_{gen}$. The compressor in the VCP side does no work directly on EVP1 which only increases the kinetic energy of the evaporated vapour from EVPI which drives cooling in the VAS side for EVP2. The COP for the VAS side is defined in Eq. (9).

$$COP_{VAS} = \frac{Q_{EVP2}}{\dot{m}_{17}(h_{18} - h_{17})} \tag{9}$$

$$\text{The overall } COP_{overall} = \frac{Q_{EVP1}}{\dot{m}_{13}(h_{13}-h_{10})} + \frac{Q_{EVP2}}{\dot{m}_{17}(h_{18}-h_{17})} \tag{10}$$

Where $\dot{m}_{17}(h_{18} - h_{17})$ is the compressor work input $\dot{W}_{comp}$ which drives cooling in the VAS side. Eqs. (8) and (9) constitute the uniqueness of the configuration and study.

2.4. Exergy Balances

The general exergy balance for a control volume in a steady state, neglecting potential, kinetic and electrical energy, is defined by Ozlu and Dincer [18] and Abam et al. [19].

$$\dot{E}_{xd} = \sum_{k}\left(1 - \frac{T_0}{T_k}\right)\dot{Q}_k - \dot{W}_{cv} + \sum_{i}(n_i\dot{E}x_i) - \sum_{e}(n_e\dot{E}x_e) \tag{11}$$

Where $\dot{E}_{xd}$ is the exergy destruction rate, $\left(1 - \frac{T_0}{T_k}\right)\dot{Q}_k$ is the exergy flow rate accompanying heat transfer, $\dot{W}_{cv}$ is the rate of work done within the control volume, $n_i\dot{E}x_i$ and $n_e\dot{E}x_e$ is the exergy flow rate in and out of the control volume. The exergy destruction is expressed in terms of product and fuel for a specific component.

$$\dot{E}_{xD,k} = \dot{E}_{xF,k} - \dot{E}_{xPk-}\dot{E}_{xL,k} \tag{12}$$

The exergy efficiency,ψ_k, and the exergy destruction ratio is equally defined for the k^{th} component as:

$$\psi_k = \frac{\dot{E}_{xPk}}{\dot{E}x_{F,k}} \tag{13}$$

$$Y_{D,k} = \frac{\dot{E}_{xD,k}}{\dot{E}_{xF,total}} \tag{14}$$

2.5. Model Validation

The present study is validated by comparing the results obtained with that interrelated theoretical simple combined power and cooling ORC system at some aspect for the topping cycle only. **Table 1** displays the comparison between the results and the studies Bejan et al. [20] and Zare et al. [21]. Using R245fa as working fluids, with ORC turbine inlet temperature at 433 K, turbine inlet pressure (TIP) at 25 bar with turbine mass flow rate at 0.5772 kg/s, the variations in percentage difference were calculated at 2.73% for energy efficiency and 1.59% for exergy efficiency when compared with the study [21]. However, an improvement potential in power output of approximately 7.92% and 36.28% was achieved when compared with those of Bejan et al. [20] and Zare et al. [21], respectively. At a generating temperature and pressure of 327 K and 4.5 bar, the bottoming vapour absorption system was compared to the study. The COPs and the cooling rate for the current study have shown a twofold performance improvement despite the same input parameters. This improvement is attributed to the modification in the thermodynamic pathways for the model SORCAS.

Table 1. System validation (SORCAS)

Parameters	[20]	[21]	[22]	Current study
ORC Turbine output (kW)	15.64	24.54	-	26.65
ORC TIT (K)	433	433	-	433
Energy efficiency (%)	14.47	37.57	-	38.63
Exergy efficiency (%)	35.47	41.46	-	42.09
Working fluid	-	-	NH_3-H_2O	NH_3-H_2O
COP (VAS)	-	-	0.256	0.643
Evaporator cooling rate (EVP1) kW	-	-	342.9	679.1
Evaporator cooling rate (EVP2) KW	-	-	926.2	679.1
Total evaporator cooling rate (kW)	-	-	1269	1358

3. Results and Discussion

3.1. Inputs and flow thermodynamic Parameters for SORCAS

The thermodynamic analysis is performed on SORCAS based on the heat input from the solar radiation in **Figure 2** and the operating conditions discussed elswhere [18], [21], [22]. **Figure 2** shows the monthly mean temperature and solar radiation for Calabar, Nigeria and the site under consideration. The location's temperature ranged between 28.13 and 33.35 °C, with solar intensity ranging between 11.64 and 16.37 MJ/m^2/day. The heat intensity generated was sufficient to raise the temperature of the low boiling point refrigerant to cause an expansion in the operational ORC turbine. On average, the amount of heat generated at all periods of the year was sufficient to run the proposed system. Furthermore, as shown in **Figure 3**, the thermodynamic state point conditions were ascertained from the operational parameters [18], [21]–[23]. From **Figure 3**, the exergy flow rate (EFR) increased from 134 to 182.9 kW for state points 23 and 24, indicating that the NH_3-H_2O solution leaving the absorber has high thermal energy required to enhance dissociation in the generator. Low entropy changes were obtained within the two states' conditions, estimated at 35% compared with entropy change of over 70% [23]. The latter is due to system configuration and operating parameters. After separation of the NH_3-H_2O in the generator, pure ammonia fluid at state 14 exits the generator at 4.7 bar with an EFR of 109 kW. The fluid was condensed at constant pressure with an increased EFR of 150 kW. The increase was due to the large difference existing between $\dot{m}(h - h_0)$ and $T_0(s - s_0)$ coupled with the high mass flow rate, $\dot{m}$. The condensate was throttled with a slight reduction in ERF of approximately 1.9%. ERF value of 150kW was evaporated in the VCP, providing cooling at state 16 (**Figure 1**).

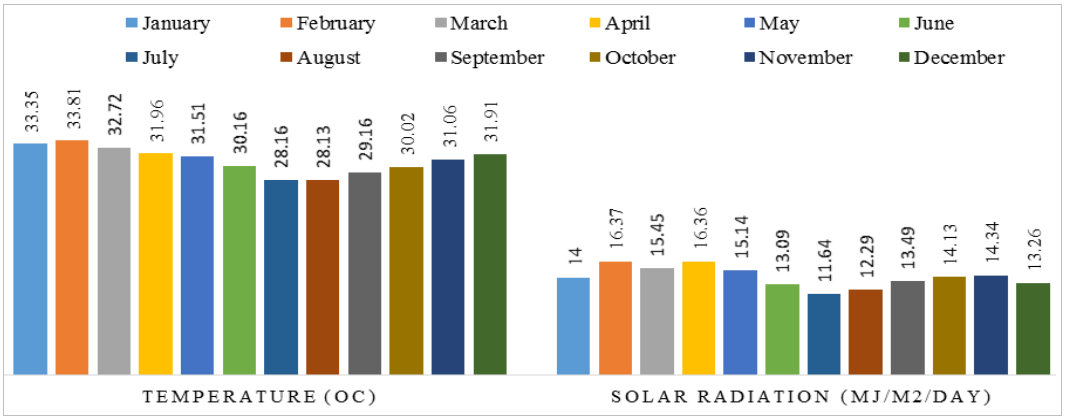

Figure 2. Monthly average temperature and solar radiation data for Calabar

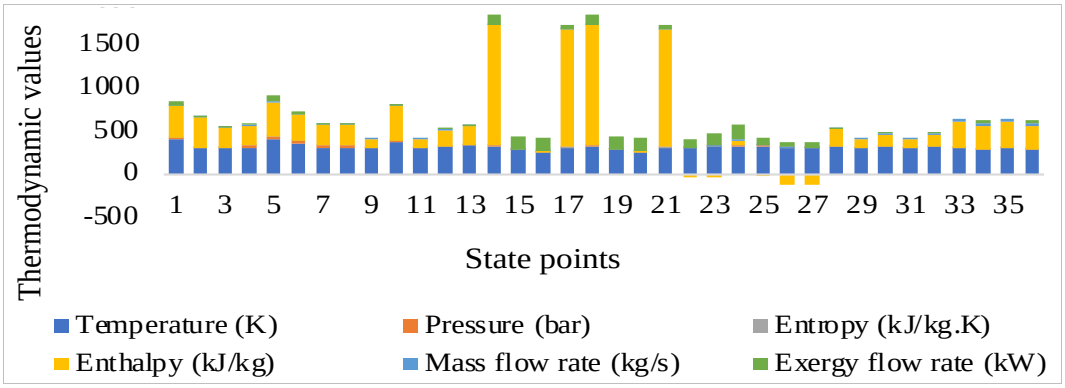

Figure 3. Thermodynamic state point characteristics in line with Figure1

3.2. Performance Based on Operating Parameters

The performance of SORCAS is demonstrated under the input parameters or operational conditions found in [18], [21], [22]. The T-S diagram for the working fluid (R245fa) [21] used in the topping ORC system is presented in **Figure 4**. The working temperatures and pressures are below the critical values of the working fluid. Thus, the system can perform optimally under these conditions. The results indicate that the turbine output in the topping ORC was calculated at 29.65 kW at parabolic collector heat input and efficiency of 351 kW and 80%, respectively. The energy and exergy efficiencies for the ORC topping cycle were 21.44 and 45% in that order. However, the overall energy and exergy efficiencies, which included the bottoming cycles, were not greater than 36.75% and 42%, respectively. The COP for the VCP was 1.77, while that for the VAS cycle was determined at 0.66. Similarly, the energy and exergy of cooling at the operating parameters were calculated at 1355 kW and 225.8 kW, respectively. The latter was based on the generator input of 96.59 kW, culminating in evaporator cooling rate of 679. 1 kW for both VCP and the VAS. The overall COP of the SORCAS was recorded at 1.844 kW, which an improvement from results was obtained elsewhere [21] and [22].

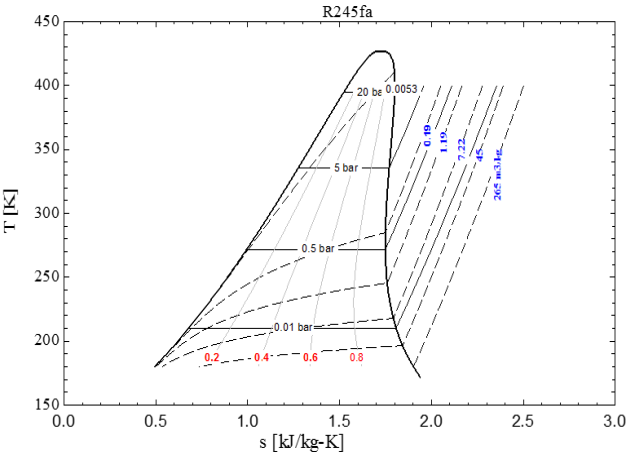

Figure 4. Temperature-entropy graph for R245fa

3.3. Parametric Investigations

3.3.1. Effect of turbine inlet temperature (TIT)

Figure 5a shows the effect of TIT on the energy and exergy efficiency of the SORCAS. The TIT can have an impact on the overall system performance. The condition of the bled fluid at the turbine depends on the TIT, which in turn determines the condition of the fluid delivered to the ORC vapour generator via hot water to the VAS generator. The TIT ranged from 388 to 415K. Between these ranges, the energy efficiency increased from 6.2 to 40%, while exergy efficiency increased from 29.02 to about 55% at constant mass flow rate. The results show that for each degree rise in TIT, the energy efficiency increases by 0.3% while the exergy efficiency increases by 0.41%. It can also be observed that the exergy efficiency values are higher than the energy efficiency. The reason for the phenomenon is depicted in **Figure 5b**. As the TIT increases, the total exergy input decreases while the turbine output (TOP) increases. For a fixed TOP, $Q_{input,total} > Ex_{input\ total}$ thus resulting in high exergy efficiency.

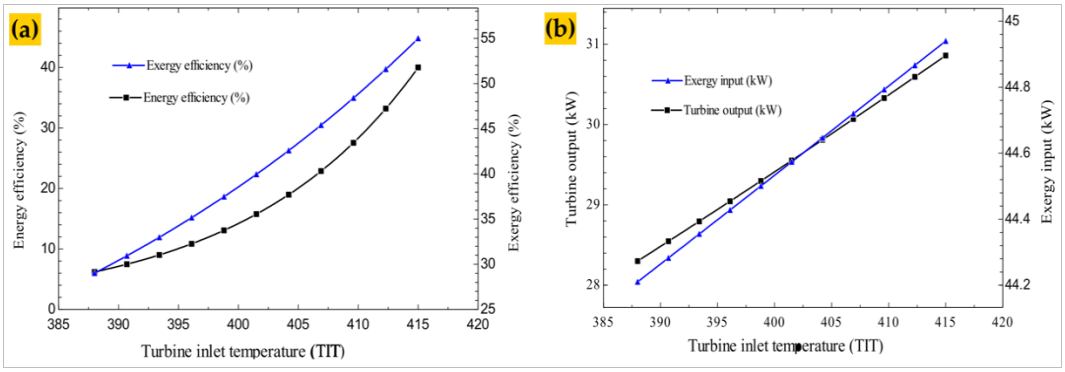

Figure 5. (a) Effect of turbine inlet temperature (TIT) on energy and exergy efficiencies; (b) Effect of turbine inlet temperature (TIT) on turbine output and exergy input

3.3.2. Effect of mass flow rate of heat transfer fluid $(\dot{m}_5)$

The effect of $\dot{m}_5$ from the receiver of the parabolic collector was investigated. **Figure 6a** shows the effect of $\dot{m}_5$ on the overall system energy and exergy efficiencies. The $\dot{m}_5$ was varied between $2.103 \leq \dot{m}_5 \leq 4.341 kg/s$, and within this range, the energy and exergy efficiencies increased by 61.05% and 61.062%, respectively. The effects of $\dot{m}_5$ on the efficiencies of the SORCAS plant was

minimal as the efficiency gap was not greater than 0.012%. Similarly, **Figure 6a** depicts the effect of $\dot{m}_5$ on the TOP and exergy output at constant (TIT). Both the TOP and exergy output increase with an increase in $\dot{m}_5$. The small enthalpy and entropy changes with a high mass flow rate were responsible for this increment.

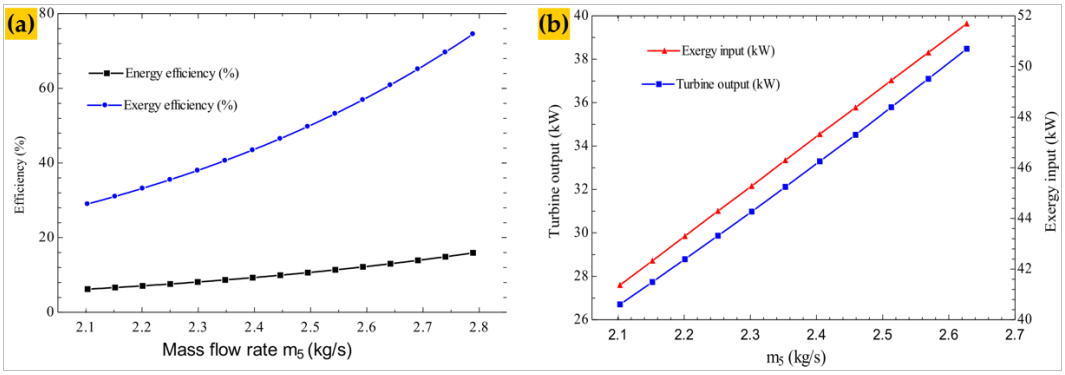

Figure 6.
(a) Effect of mass flow rate of heat transfer fluid (m ̇_5) on energy and exergy efficiencies; (b) on exergy input and turbine output

3.3.3. Effect of generator temperature

The effect of generator temperature on the total cooling rate and exergy of cooling is presented in **Figure 7a**. While the impact of temperature on COP is shown in **Figure 7b**. From **Figure 7a**, the total cooling rate increases for an increasing temperature of the VAS generator. The total cooling rate increased from 1086 kW to 3259 kW, with a 1.73% rise in VAS generator temperature. Similarly, at the same temperature rise, the exergy of cooling decreases by about 1.56%. The enthalpy changes for the NH_3-H_2O increases for a constant mass flow rate and pressure, leading to high refrigerating effects (**Figure 7a**). Also, increasing generator temperature at constant mass flow rate may result to small enthalpy difference because of high inlet and outlet enthalpies. This may result to reduction in Q_{gen} leading to the increase in the COP of the VCP side. Similarly, since the same condensate mass flow rate from the VCP is throttled at a very minimum temperature change, the enthalpy variation remains insignificant, thus maintaining the same refrigerating effect in the VAS side as the ratio $\frac{Q_{EVP1}}{\dot{W}_{comp}}$ increases due to the reduction in $\dot{W}_{comp}$.

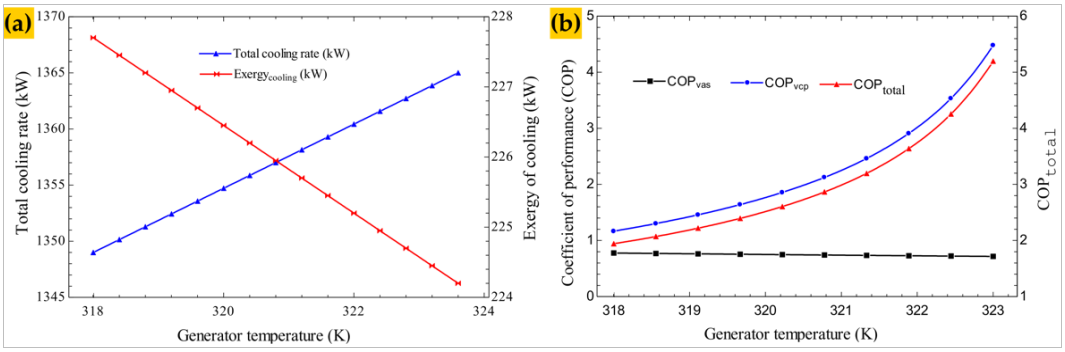

Figure 7.
(a) Effect of generator temperature on cooling rate and exergy of cooling; (b) coefficient of performance

3.3.4. Effect of generator pressure on performance parameters

Table 2 depicts the effects of change in generator pressure on COP, exergy destruction (ED), heat load, energy, and exergy of cooling. The study considered generator pressure ($P_{generator}$) between 4.75 and 4.95 bar. Within this pressure range, the COP increases from 1.984 to 3.046 bar at a constant generator temperature of 321 K. The increase in COP is attributed to the reduction in the generator heat rate (Q_{gen}), which decreases from 90.81 kW at 4.75 bar to 62.89 kW at 4.95 bar. Similarly, the increase in P_{gen} reduces the compressor work in the VCP system by about 2.44%. The reduction in the generator heat rate (Q_{gen}), led to the rise in the COP of the VCP system from 1.322 to 2.405. However, the COP_{VAS} decreases across the pressure range by about 3.03%. The decline in the COP_{vas} is attributed to the constant mass flow rate from the EVP_1 to EVP_2 and little differential enthalpies ranges. Nonetheless, the study has attempted to obtain a comparable cooling rate in the VCP and VAS sides using the same condensate. Consequently, this increased the overall cooling rate (energy of cooling) and the COP. The latter was achieved through the selection of operating parameters and has been considered notable in this study. Additionally, the exergy destruction rate (EDR) of the components that are directly affected by the variations in the P_{gen} of

the bottoming VAS system are equally presented in Table 2. The EDR decreases slightly in some components with the increase in P_{gen}. The reason is ascribed to the following: high source temperature and constant mass flow rate, decrease in the generator thermal load, and the decrease in the physical exergy change of the streams.

Table 2. Effect of VAS generator pressure performance parameter and component systems (at T_{gen} = 321 K)

Results	P_{gen} = 4.75 (bar)	P_{gen} = 4.80 (bar)	P_{gen} = 4.85 (bar)	P_{gen} = 4.90 (bar)	P_{gen} = 4.95 (bar)
$Q_{Generator}$ (kW)	90.81	84.64	78.01	70.81	62.89
$QEVP_1$ (kW)	678	677	676	675	674
$QEVP_2$ (kW)	678	677	676	675	674
VAS_{exergy} cooling	1356	1354	1352	1350	1348
VAS_{exergy} cooling	225.7	225.7	225.6	225.5	225.4
$W_k$comp	14.81	14.91	15.00	15.09	15.18
COP_{vcp}	1.322	1.50	1.722	2.01	2.405
COP_{vas}	0.661	0.656	0.651	0.6459	0.641
Overall COP	1.984	2.156	2.373	2.656	3.046
E_DGenerator	15.62	15.62	15.62	15.62	15.62
E_DEVP_1	86.53	86.53	86.53	86.52	86.52
E_DEVP_2	86.53	86.53	86.53	86.52	86.52
E_DPUMP 2	0.00925	0.00925	0.00931	0.00931	0.00932
E_DAbsorber	4.624	4.505	4.387	4.270	4.154
E_DCON 2	54.27	53.57	53.57	52.17	51.49
E_DCON 3	54.27	53.57	53.57	52.17	51.49
E_DVAS HEX	22.04	21.29	20.56	19.86	19.18

3.3.5. Exergy destruction ratio, exergy of fuel /product and improvement potential

Table 3 presents some thermodynamic performance indicators, such as exergy of fuel ($\dot{E}_F$), the exergy of product ($\dot{E}_P$) exergy ratio ($Y_{D,k}$), exergy destruction ratio of the component system (Y^*_{Dk}) and the exergetic improvement potential (IP). The components efficiencies are also presented in Table 3, and the parameters were calculated at operating conditions. Eq. (15) expresses the IP as calculated from [24], [25]. The IP locates areas with a high prospective for improvement in a thermal process.

$$IP = (1-\psi)\left(\dot{E}_{in} - \dot{E}_{out}\right) \tag{15}$$

Where ψ denotes exergy efficiency, $\dot{E}_{in}$ and $\dot{E}_{out}$ represent the exergy in and out of the system, respectively.

$\psi = \frac{\dot{E}_{out}}{\dot{E}_{in}}$, then, Eq. (15) can be presented as:

$$IP = (1-\psi)^2 \times \dot{E}_{in} \tag{16}$$

Table 3 further shows that certain components, such absorbers, evaporator, generators, valves, and pumps, have higher total fuel exergy. The total fuel exergy was 1.7 times higher than the product exergy, indicating that 58.34% of the real exergy was used to power the thermal plant, with the remaining 41.66% of the quality exergy being lost due to system irreversibilities. It can be inferred that the overall exergy of the plant is 58.34%, which differs from the 42.09% exergy efficiency calculated earlier in this study (Table 1). The reason is that the 58.34% efficiency obtained excluded the irreversibilities within the solar unit. However, the total IP was calculated at 426.768 kW with the absorber, VAS HEX, evaporators, VAS pump 2, and ORC pump 3 contributing about 27.97%, 15.92%, 15.54%, 5.84% and 4.33%, respectively. The absorber, VAS HEX and the cooling evaporators have the highest prospect for improvement, followed by ORC and the VAS pumps. For the pumps, the dimensions of the condensers must be adjusted during design to ensure complete condensate at the end state. The latter will allow the pump to handle pure liquid rather than a vapour mixture. In the absorber, the disparity in temperature between the vapour and fluid is high. Thus, a large entropy difference exists, which results in high irreversibilities. However, in design consideration, fluid selection and concentration, pressure and temperature variations are paramount in designing an effective absorber.

Table 3. Exergy destruction ratio, exergy of fuel product and improvement potential

Components	$\dot{E}_F$(kW)	$\dot{E}_P$(kW)	$Y_{D,k}$	Y^*_{Dk}	$\psi_k = \frac{\dot{E}_P}{\dot{E}_F}$ (%)	IP (kW)
ORC turbine	29.65	11.32	0.007429	0.01568	38.18	11.33
ORC condenser 1	1.536	1.436	0.004168	0.008795	93.49	0.00651
Condenser 2	43.60	3.10	0.05303	0.1119	7.11	37.62
ORC VG	44.08	28.47	0.01506	0.03179	64.59	5.528
VAS VG	221.294	197.49	0.08679	0.1831	89.24	2.561
WHT	16.71	12.730	0.003843	0.08109	76.18	0.948
VAS HEX	149.91	48.88	0.0219	0.04638	32.61	68.08
ORC Pump 1	9.88	2.616	0.000004812	0.00001015	26.48	5.34
ORC Pump 3	18.69	0.11	0.000007425	0.00001567	0.5886	18.47
VAS Pump 2	90.88	43.270	0.00000892	0.00001882	47.61	24.94
Valve 1	153.1	150.00	0.002995	0.00632	97.98	0.06262
Valve 2	61.92	58.54	0.003258	0.006876	94.54	0.1845
Valve 3	153.00	150.30	0.002908	0.006137	98.24	0.04752
Absorber	127.96	25.36	0.06972	0.1471	3.407	119.4
Evaporator 1	112.92	26.38	0.08344	0.1761	23.36	66.32
Evaporator 2	112.78	26.38	0.08344	0.1761	22.95	65.93
Total	**1347.91**	**786.382**	**0.5135**	**0.997**	-	**426.768**

4. Conclusion

The study proposed and appraised a solar-driven combined power and cooling system with bottoming vapour compression absorption refrigeration cycles using NH_3-H_2O as the thermodynamic working fluid. The refrigeration sub-system consists of two cooling evaporators to produce an equivalent cooling effect using the condensate from one evaporator. Additionally, to demonstrate the system's thermodynamic viability, a parametric study was conducted to observe the performance at certain thermodynamic variations and the results are summarized as follows: The energy and exergy efficiencies for the ORC topping cycle were 21.44 and 45%, respectively. While the overall efficiencies, including the bottoming cycles, were 36.75% for energy and 42% for exergy. The variations in the mass flow rate of the heat transfer fluid ($\dot{m}_5$) range between $2.103 \leq \dot{m}_5 \leq 4.341 \text{kg/s}$ led to a slight increase in the energy and exergy efficiency with about a 0.012% efficiency gap. The overall cooling rate (CR) increases for increasing generator temperature by 1.73%, with a maximum CR of 3259 kW obtained at 320 K. Also, at the same temperature rise, the exergy of cooling decreases by approximately 1.56%. The overall COP increases from 1.984 to 3.046 at a constant generator temperature of 321 K. The increase in COP is attributed to the reduction in the generator heat rate, which decreases as the pressure increases. The overall exergy of fuel was 1.7 times greater than that of the product, while 41.66% was lost, with only 58.34% utilized to drive the system. The total improvement potential was calculated at 426.768 kW with the absorber, VAS HEX, evaporators, VAS pump 2, and ORC pump 3 contributing approximately 27.97%, 15.92%, 15.54%, 5.84% and 4.33%, respectively and equally have the highest potential for improvement.

Authors' Declaration

Authors' contributions and responsibilities - The authors made substantial contributions to the conception and design of the study. The authors took responsibility for data analysis, interpretation, and discussion of results. The authors read and approved the final manuscript.

Funding –No funding information from the authors.

Availability of data and materials - All data is available from the authors.

Competing interests - The authors declare no competing interest.

Additional information – No additional information from the authors.

References

[1] R. V. Padilla, G. Demirkaya, D. Y. Goswami, E. Stefanakos, and M. M. Rahman, "Analysis of power and cooling cogeneration using ammonia-water mixture," *Energy*, vol. 35, no. 12, pp. 4649–4657, 2010, doi: 10.1016/j.energy.2010.09.042.

[2] K.-H. Kim, "Thermal analysis of a combined absorption cycle of cogeneration of power and cooling for use of low temperature source," *Korean Journal of Air-Conditioning and Refrigeration Engineering*, vol. 23, no. 6, pp. 413–420, 2011.

[3] J. Wang, J. Wang, P. Zhao, and Y. Dai, "Thermodynamic analysis of a new combined cooling and power system using ammonia–water mixture," *Energy Conversion and Management*, vol. 117, pp. 335–342, 2016, doi: 10.1016/j.enconman.2016.03.019.

[4] D. Y. Goswami, "Solar thermal power: status of technologies and opportunities for research," *Heat and Mass Transfer*, vol. 95, pp. 57–60, 1995.

[5] D. Y. Goswami, "Solar thermal power technology: present status and ideas for the future," *Energy sources*, vol. 20, no. 2, pp. 137–145, 1998, doi: 10.1080/00908319808970052.

[6] D. Y. Goswami and F. Xu, "Analysis of a new thermodynamic cycle for combined power and cooling using low and mid temperature solar collectors," *Journal of Solar Energy Engineering*, vol. 121, no. 2, pp. 91–97, 1999, doi: 10.1115/1.2888152.

[7] F. Xu, D. Y. Goswami, and S. S. Bhagwat, "A combined power/cooling cycle," *Energy*, vol. 25, no. 3, pp. 233–246, 2000, doi: 10.1016/S0360-5442(99)00071-7.

[8] K. H. Kim, G. Kim, and C. H. Han, "Performance assessment of ammonia-water based power and refrigeration cogeneration cycle," *International Journal of Materials, Mechanics and Manufacturing*, vol. 1, no. 1, 2013, doi: 10.7763/IJMMM.2013.V1.8.

[9] Z. Yu, J. Han, H. Liu, and H. Zhao, "Theoretical study on a novel ammonia–water cogeneration system with adjustable cooling to power ratios," *Applied energy*, vol. 122, pp. 53–61, 2014, doi: 10.1016/j.apenergy.2014.02.010.

[10] X. Jing and D. Zheng, "Effect of cycle coupling-configuration on energy cascade utilization for a new power and cooling cogeneration cycle," *Energy conversion and management*, vol. 78, pp. 58–64, 2014, doi: 10.1016/j.enconman.2013.10.038.

[11] J. Hua, Y. Chen, Y. Wang, and A. P. Roskilly, "Thermodynamic analysis of ammonia–water power/chilling cogeneration cycle with low-grade waste heat," *Applied thermal engineering*, vol. 64, no. 1–2, pp. 483–490, 2014, doi: 10.1016/j.applthermaleng.2013.12.043.

[12] L. Sun, W. Han, D. Zheng, and H. Jin, "Assessment of an ammonia–water power/cooling cogeneration system with adjustable solution concentration," *Applied thermal engineering*, vol. 61, no. 2, pp. 443–450, 2013, doi: 10.1016/j.applthermaleng.2013.08.026.

[13] L. Sun, W. Han, X. Jing, D. Zheng, and H. Jin, "A power and cooling cogeneration system using mid/low-temperature heat source," *Applied energy*, vol. 112, pp. 886–897, 2013, doi: 10.1016/j.apenergy.2013.03.049.

[14] W. Han *et al.*, "Experimental studies on a combined refrigeration/power generation system activated by low-grade heat," *Energy*, vol. 74, pp. 59–66, 2014, doi: 10.1016/j.energy.2014.02.097.

[15] R. Shankar and T. Srinivas, "Investigation on operating processes for a new solar cooling cogeneration plant," *Journal of solar energy engineering*, vol. 136, no. 3, p. 31016, 2014, doi: 10.1115/1.4027423.

[16] L. C. Mendoza, D. S. Ayou, J. Navarro-Esbrí, J. C. Bruno, and A. Coronas, "Small capacity absorption systems for cooling and power with a scroll expander and ammonia based working fluids," *Applied thermal engineering*, vol. 72, no. 2, pp. 258–265, 2014, doi: 10.1016/j.applthermaleng.2014.06.019.

[17] J. López-Villada, D. S. Ayou, J. C. Bruno, and A. Coronas, "Modelling, simulation and analysis of solar absorption power-cooling systems," *International journal of refrigeration*, vol. 39, pp. 125–136, 2014, doi: 10.1016/j.ijrefrig.2013.11.004.

[18] S. Ozlu and I. Dincer, "Development and analysis of a solar and wind energy based multigeneration system," *Solar Energy*, vol. 122, pp. 1279–1295, 2015, doi: 10.1016/j.solener.2015.10.035.

[19] F. I. Abam *et al.*, "Exergoeconomic and environmental modeling of integrated polygeneration power plant with Biomass-Based syngas supplemental firing," *Energies*, vol. 13, no. 22, p. 6018, 2020, doi: 10.3390/en13226018.

[20] H. Rostamzadeh, M. Ebadollahi, H. Ghaebi, M. Amidpour, and R. Kheiri, "Energy and exergy analysis of novel combined cooling and power (CCP) cycles," *Applied Thermal Engineering*, vol. 124, pp. 152–169, 2017, doi: 10.1016/j.applthermaleng.2017.06.011.

[21] F. I. Abam *et al.*, "Thermoeconomic and exergoenvironmental sustainability of a power-cooling organic Rankine cycle with ejector system," *e-Prime-Advances in Electrical Engineering, Electronics and Energy*, vol. 2, p. 100064, 2022, doi: 10.1016/j.prime.2022.100064.

[22] M. Higa, E. Y. Yamamoto, J. C. D. de Oliveira, and W. A. S. Conceição, "Evaluation of the integration of an ammonia-water power cycle in an absorption refrigeration system of an industrial plant," *Energy Conversion and Management*, vol. 178, pp. 265–276, 2018, doi: 10.1016/j.enconman.2018.10.041.

[23] A. H. Mosaffa, L. G. Farshi, and S. Khalili, "A novel enhanced ammonia-water power/cooling cogeneration system with dual level cooling temperature: Thermodynamic and economic assessments," *Energy Conversion and Management*, vol. 244, p. 114530, 2021, doi: 10.1016/j.enconman.2021.114530.

[24] F. I. Abam *et al.*, "Projection of sustainability indicators, emissions and improvement potential of the energy drivers in the Nigerian transport sector based on exergy procedure," *Scientific African*, vol. 16, p. e01175, 2022, doi: 10.1016/j.sciaf.2022.e01175.

[25] T. Chowdhury *et al.*, "A case study to application of exergy-based indicators to address the sustainability of Bangladesh residential sector," *Sustainable energy technologies and assessments*, vol. 37, p. 100615, 2020, doi: 10.1016/j.seta.2019.100615.